

Transport properties of continuous quantum walks on fixed graphs

Michele Valotti

Level 4 Project, MPhys Physics

Supervisors: Dr Vivien Kendon and Dr Nicholas Chancellor

Department of Physics, Durham University

Submitted: April 19, 2019

Random walks have been the subject of great interest in many areas of science. Their quantum counterpart, quantum random walks, have been shown to have many potential applications. In this paper their transport properties on different types of fixed graphs are studied, focusing on continuous quantum walks. Other effects such as asymmetrical potentials, decoherence and particle interactions are modelled for a simple graph. A theoretical framework for the dynamics of quantum particles on various lattices is a useful ideal model to be compared to experimental results, and in this work it is applied to square lattices, carbon nanotubes and graphs with a high degree of clustering. The results from the simulation of nanotubes show that this model can replicate their transport properties despite not directly accounting for their electrical properties. Results from random graphs show the importance of a regular structure and high connectivity for fast quantum transport.

Contents

1. Introduction	2
2. Quantum walks on the line	4
A. Coined quantum walk	5
B. Continuous quantum walk	7
3. Square lattices	9
A. Introducing additional effects	10
B. Measuring transport properties	14
4. Hexagonal lattices	16
A. Carbon nanotubes	18
5. Cluster Lattices	22
A. Random clusters	22
B. Hexagonal clusters	26
6. Conclusions	28
Acknowledgments	28
References	28

1. INTRODUCTION

The study of random walks has been of great interest to many fields since the term was first coined in 1905 by Karl Pearson [1]. A random walk is a stochastic process that describes the trajectory of a walker taking random steps in a space. This behaviour can be observed in many phenomena of nature and in some human activities. Examples include the motion of gaseous molecules, the fluctuations of trading stocks, or the movements of bacteria searching for food. The classical random walk can be considered a special case of a Markov chain, a model for a stochastic process where every event is only influenced by the event that precedes it [2]. A Markov chain is often defined in a countable state space, and in either discrete or continuous time [3]. This is what is of most interest for this work, as the walks that will be considered will evolve on a discrete lattice. Classical random walks, however, are not only an interesting model of our reality, but they have also been exploited in the field of computer science, where they have great applications in the design and realization of powerful algorithms. Deemed a cornerstone of computer science [4], random walks have been applied to central problems by virtue of their ability to sample and explore combinatorial structures [5]. The way they are applied to these problems is by sampling from a graph whose distribution is the same as the limiting distribution of the random walk [5]. The speed at which the walk approaches the limiting distribution then becomes crucial to the speed of the algorithm. In the search for ever increasing efficiency, and in the constant struggle to keep up with Moore's Law [6], computer scientists and engineers have veered away from the classical world and ventured into the quantum realm. After coming to terms with the reality that our world is in fact quantum, and cannot be fully described by the more intuitive Newtonian mechanics, the field of quantum mechanics has evolved to exploit its unusual behaviours. Today new technologies take advantage of the counter-intuitive qualities of non classical phenomena, and apply them to ideas such as quantum cryptography [7], quantum computation and quantum simulation. The most famous example is probably Shor's algorithm [8], first formulated in 1995, which would allow to factorise prime numbers in polynomial time, effectively breaking modern encryption. The idea of quantum computers, however, predates Shor by more than 10 years, and was imagined by Richard Feynman [9], who argued that a reality that is unequivocally quantum can only be simulated by a quantum system. This idea has spawned the field of quantum computing, which has developed greatly in recent years and has managed to overcome incredible theoretical and engineering challenges, yet remaining far from having reached its full potential. With many algorithms being studied on the theoretical side of quantum computing, the hardware struggles to innovate at the same speed, but some proofs of concept of what advantages a quantum computer could bring have already been achieved. One of the notable examples is IBM, that built a simple quantum computer [10] and has successfully modelled interactions between atoms in a complex molecule [11]. As mentioned before, random walks play a very important role in the development of algorithms in a classical computer, sparking an interest in their quantum counterpart, and its effectiveness in a quantum setting. One of the most famous applications of quantum random walks is known as quantum search, the concept of which was introduced by Grover [12], who proved that exploiting the effects of a quantum walk, his algorithm could find a target value in an optimal number of queries \sqrt{N} . This brings a quadratic improvement over classical search. It has become clear that quantum random walks are of great interest for the field of quantum computation, both in the development of

quantum algorithms and in the study of quantum simulations. It therefore becomes important to study their properties, in order to understand their behaviour and devise new applications, as well as identify their limitations.

Classical random walks are often described with the aid of a "walker and coin" metaphor, where a walker on a graph (in the simplest case a line) moves one step in the direction determined by the side on which the coin lands. The throw introduces not only the random character of the walk, but also its discreteness, moving the walker one step for each throw. It is natural then, when trying to formulate the quantum equivalent of a random walk, to start from the same elements of the classical one, and add the quantum effects to one of its elements. This was the case for the first kind of quantum random walk that was formulated, initially by Feynman [13] and then rediscovered in the field of quantum computing by Meyer [14]. The quantum effect was added to the coin, allowing it to enter a superposition of its possible state, leading to unique interference effects in the path of the walker. This model takes the name of discrete or coined quantum walk, but it is not the only description of random walks in a quantum setting. In 1998 Farhi *et al.* [15] devised a new model for quantum walks that removed the coin from the system, and more closely resembles Markov chains. This new model, which takes the name of continuous quantum walk, has the advantage of taking place solely in the position space of the walker, instead of being augmented by the state space of the coin, as it is in the case of discrete quantum walks. Despite seeming different, these two models have been shown to give similar results for the same graph, and being equivalent for the walk on the line [16]. The mathematical description of these two models will be outlined in the following section of this report. This work, however, will be focused on the behaviour of continuous quantum walks on different graphs, as these provide a simpler framework for computer simulations, despite requiring numerical integration, which could lead to approximation errors. Due to the size and length of the simulations in this work, however, this concern was set aside, in favour of a mathematical framework that could more easily be adapted to different graphs and represent a more conceptually simple model of transport [17]. Despite their similarities, coined and continuous quantum walks do not always lead to the same results: while discrete quantum walks have been proved to bring a quadratic speed up in search algorithms for graphs of dimension $d \geq 2$ [18], the same cannot be said for continuous quantum walks, which require a dimension of $d \geq 4$ [19]. Although the search problem is a very interesting one, this work focuses on the dynamics of continuous walks on physical systems, and specifically on 2-dimensional lattices. This precluded the study of search, as it would not have led to a useful speedup. Interesting studies on continuous quantum walk search have been conducted by Foulger, Gnutzmann and Tanner [20], using a graphene lattice topology.

Focusing on the dynamics of quantum random walks alone, without investigating their role in quantum algorithms such as search, might seem a very abstract approach to the problem. The aim of this work, however, remains to build a useful framework to gain helpful insight into a process that has only been analytically solved for special cases [21]. Building a simulation of the dynamics of a quantum particle on various types of graphs provides a simple model of complicated physics, where all the parameters can be tuned, and the simulated results can be compared to the experimental ones. This provides the great advantage of having perfect control of many variables, such as tunable decoherence, size and shape of the graph on which the particle evolves, and the interaction between the particle and the graph. In this way useful

comparisons between different lattice structures can be made, and any effects of unexpected physics which would arise in an experimental setting can be avoided. Exploring the simple dynamics of a particle can be the first step to lead to a deeper understanding of the physics behind the quantum algorithms of the future, as well as that of many other applications. It is therefore important to build a model that allows us to investigate the properties of these physical phenomena: quantum random walks are a good model of the dynamics of quantum objects moving on a lattice. The isomorphism between quantum transport on spin chains and continuous quantum walks has been proven by Bose [22], but in this work the simulations focus on continuous quantum walks in 2 dimensions, building up from a simple square lattice to more complicated graphs with various degrees of randomness. The comparison between lattices will be drawn with respect to the transport properties of the same particle on different graph structures, paying particular attention to the spreading of the quantum walker (calculated through its standard deviation) and what will be defined as its arrival probability. Additional effects such as decoherence and the interaction between two particles will be mentioned, as it constitutes part of the useful framework that will be built in this work, but the focus of the report will remain on the simple dynamics of a particle. Simulated structures include a simple square graph, a hexagonal lattice, and different types of cluster graphs. Where the square graph is not of much physical relevance, and serves more as a proof of concept for the model, the hexagonal graph can draw useful comparisons to structures like graphene and carbon nanotubes, while the cluster graphs are more similar to magnetic domains or microcrystalline structures.

The report will be organised as follows. The fundamental mathematics behind a quantum walk will be outlined in section 2, with examples of a 1-dimensional coined quantum walk and of its continuous counterpart. In section 3, 2-dimesional continuous quantum walks will be presented, examining their transport properties, and introducing some simple models for adding a potential, the effects of interactions with a second particle and decoherence. In section 4 the focus will move to hexagonal lattices and carbon nanotubes. Finally, in section 5, the results of various types of cluster graphs will be shown, and compared to previous results.

2. QUANTUM WALKS ON THE LINE

A classical random walk takes a walker on a graph and moves it to the next node in the direction that is determined randomly by the toss of a coin. In the simplest example of a classical random walk the position space is 1-dimensional, i.e. a line, and the walker moves left or right if the coin toss results in heads or tails. If we observe a random walker, and note its position after n throws, we will find that, after many trials, the probability distribution of its final positions will be binomial, and its average distance from its starting position will be \sqrt{n} . The standard deviation of a classical random walk on a line is therefore proportional to the square root of the number of steps taken by the walker. This is a measure of how quickly a walker spreads on a certain graph and it will be used to compare the classical and quantum versions of random walks. Random walks have been extensively studied in their classical setting and some examples can be found in [23][24][25]. The key idea behind a quantum random walk is to drive the evolution with a unitary (reversible) operator without any intermediate measurements [26]. Many of the unexpected behaviours of a quantum walker are due to its delocalization

and consequent interference effects. Here a description of the mathematical model behind the two flavours of quantum walks will be given, but all the results will be simulated, rather than obtained analytically.

A. Coined quantum walk

The more intuitive way to transition between classical and quantum random walks is to introduce one of the most fundamental quantum effects into the phenomenon: superposition. If the classical walker follows all the possible classical paths in a superposition, we will have obtained a quantum version of the random walk. As it often is in quantum mechanics, however, the most intuitive solution is not the right one, as it was proved by Meyer [14]. This superposition, in fact, would make the walk non-reversible (i.e not unitary), and therefore not physical in a quantum mechanical setting. The way to add quantum mechanical effects to the random walk is therefore to introduce a quantum coin. The quantum system is now comprised of a quantum coin and a conditional shift operator that acts according to the state of the coin [27]. At each step the walker throws the quantum coin and is shifted left or right according to the state in which the coin is. This is where the quantum effects come into play, as the coin can be found in a superposition of its two states. The walker is evolved for n timesteps and measured at the end of its evolution. The quantum measurement is where the randomness enters the system, as the probability to find the walker in a certain position is determined by the amplitude of its wavefunction. The walker lives in the position space H_p of dimension d_p where d_p is the number of positions on the line. The coin lives in the state space H_c of dimension d_c where d_c is equal to the number of edges each node on the graph has, or the number of sites the walker can jump to from its position. The walker can be initialised in any state or superposition of states on the line. The coin can be found in either of its states, or a superposition of both. The quantum system can be, for example, in state $|\psi(0)\rangle = \alpha |middle, +1\rangle + \beta e^{i\phi} |middle, -1\rangle$. In this case the walker starts in the middle and the coin starts in a superposition of its two states, out of phase by a factor ϕ . For a coined quantum walk the evolution is carried out in two steps: first the state of the coin is evolved by a toss operator C and then a conditional step operator S is applied to the walker. The toss operator can be in principle any unitary operator [28], but the general form, up to a phase $e^{i\phi}$, can be expressed as:

$$C = \begin{pmatrix} \sqrt{\eta} & \sqrt{1-\eta} \\ \sqrt{1-\eta} & -\sqrt{\eta} \end{pmatrix}, \quad (1)$$

where η is the probability of moving in one direction and $0 \leq \eta \leq 1$. For $\eta = 1/2$ the Hadamard unbiased coined $C^{(H)}$ is obtained. The step operator can be defined by its effect on the walker as:

$$S |position, coin\rangle = |position + coin, coin\rangle. \quad (2)$$

The action of the step operator is to shift the position of the walker by one step in either direction, according to the state of the coin. The operator on the total Hilbert space $H_p \otimes H_c$ is

therefore $U = S \cdot (C \otimes \mathbb{1}_d)$. This is the unitary operator that acts on the walker, which after t steps will be found in state

$$|\psi(t)\rangle = U^t |\psi(0)\rangle, \quad (3)$$

where $|\psi(0)\rangle$ is defined as before. The wavefunction remains normalised to 1 and the square modulus of its amplitude is equal to the probability of finding it in any state. Once the walker has evolved, and the unitary operator has acted on it t times, a measurement must be performed, and this is where the randomness enters the system. To observe the position of the walker an operator M_p is defined, given by:

$$M_p = \sum_i \mathbb{1} \otimes |p_i\rangle \langle p_i|, \quad (4)$$

where p_i is the pure state at position i . This operator projects the final state in the pure position states, from which we can recover the probability as the square modulus of the amplitude.

The results of the simulations for this walk on a line, shown in Fig. 1, may seem odd or counter-intuitive, but they are exactly the results that were expected. All the simulations in this work were run in *python*, with the help of libraries such as *numpy* for more mathematically advanced functions, and *matplotlib* for plotting the graphs. In this simulation a quantum walker is initialised in the middle position on the line, and the coin is in either a pure $|+1\rangle$ or $| -1\rangle$ state, or an equal superposition of the two. Thanks to the great flexibility of *python* and its libraries, it was possible to follow the mathematical formalism quite closely. The walk

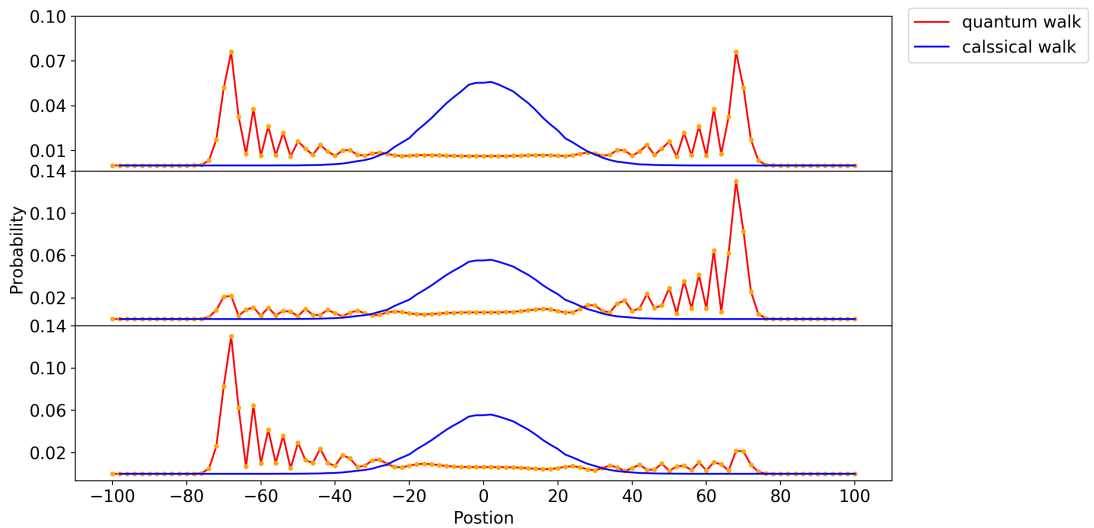


FIG. 1: Distributions shown after 100 steps. From top to bottom, the coin was initialised in a superposition of $| -1\rangle$ and $| +1\rangle$, a pure $| +1\rangle$ state and a pure $| -1\rangle$ state. The classical walk was averaged over 10000 trials. Only even points are shown.

is discretised in both space and time, hence for even times, only even positions are occupied.

The quantum walk distributions are compared to their classical counterpart and the difference is quite striking. First of all it is clear that the starting state of the quantum coin has a great effect on the final distribution, skewing it to one side and giving it a strong bias. Secondly, the spread of the quantum distribution is much larger, and does not remotely resemble the classical binomial distribution. The interference phenomena between the quantum states lead to unusual and unexpected behaviours, but ones that, especially in higher dimensions, can be and have been exploited. A useful measure for comparing different kinds of random walks is their standard deviation, defined in 1 dimension for the walk on the line, which can be interpreted as the speed at which they spread, when plotted over time. The standard deviation for the classical walk in

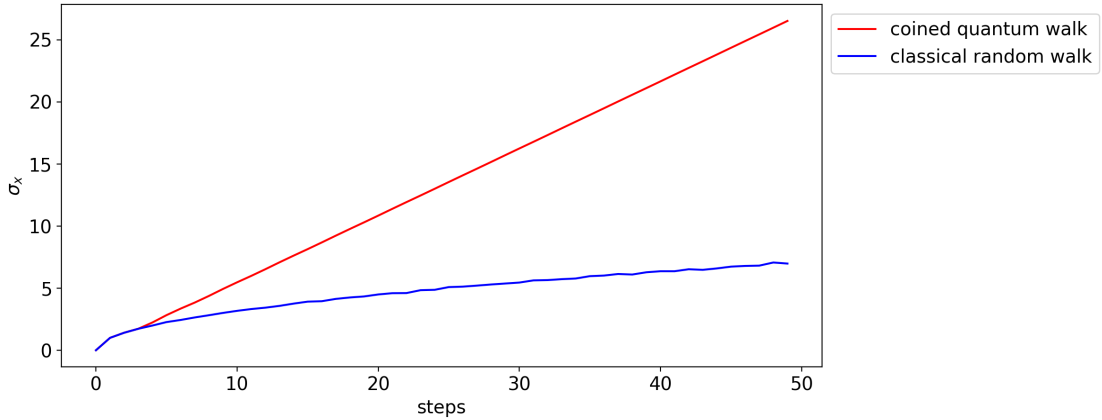


FIG. 2: One dimensional standard deviation for a coined quantum walk and a classical random walk.

Fig. 2 has the expected shape, which grows as the square root of the number of steps. The quantum walk, instead, spreads linearly, and therefore much faster. The coined quantum walk in 1 dimension has been solved analytically [29], but this example still serves as a useful proof of concept and as a helpful sanity check. Now that the model has been proven to work, and agrees with previous results, it can be compared to the walk this work is going to be focusing on. The tools developed in this section, such as the standard deviation, are still going to be used, but the walker will follow a time-continuous evolution.

B. Continuous quantum walk

The idea of continuous-time quantum walks dates back to 1964 [30] but was not formulated and applied to quantum algorithms until 1998 [15]. The intuition behind it seems very far from the coined quantum walk, but the results it leads to are remarkably similar. The main difference between the continuous and discrete quantum walk is the removal of the coin: a continuous quantum walker still evolves on a discretised space, but in a time-continuous manner, and it is not tied to the state of a quantum coin, nor to the bias that comes with it. A continuous quantum walk then exists entirely in the position Hilbert space H_p . The classical counterpart of this walk can be found in Markov chains, where the probability distribution of a classical walker evolves on a graph V according to a matrix A as:

$$\vec{p}_{t+1} = A\vec{p}_t, \quad (5)$$

where \vec{p} is the probability vector of dimension equal to the number of nodes on graph V . The entries $A_{i,j}$ of the matrix A give the probability to move from node i to node j at every time step, and are non-zero if the nodes i, j are connected. This matrix can be recognised as the adjacency matrix, which encodes the geometry of the graph it describes. For the process to be continuous in time a hopping rate γ is introduced, which represents the probability of jumping to a neighbouring node at any point in time, and Eq. (5) is turned into the differential equation:

$$\frac{d\vec{p}(t)}{dt} = \gamma(A - D)\vec{p}(t), \quad (6)$$

where D is the degree matrix with entries $D_{i,i}$ equal to the degree of node i . If the graph is a cycle, then $D = d\mathbb{1}$. The matrix $(A - D)$ is redefined as H , and the reason will become clear when considering the quantum walk. Solving Eq. (6) gives the result:

$$\vec{p}(t) = \exp(-Ht)\vec{p}(0). \quad (7)$$

Farhi and Gutmann [15] translated this classical formalism into the quantum language to describe continuous quantum walks, which remain reversible without the need of a coin. The conversion to the quantum realm is relatively simple: the generator matrix H becomes the Hamiltonian of the system, which evolves following unitary evolution according to the operator:

$$U = \exp(-iHt), \quad (8)$$

where the entries of H are determined by the geometry of the graph on which the quantum system evolves. In a continuous walk the wavefunction lives in the Hilbert space of position only, and evolves as:

$$|\psi(t)\rangle = U^t |\psi(0)\rangle. \quad (9)$$

Writing the operator U explicitly shows how it can be factorised: since the adjacency matrix A commutes with the degree matrix D and $U = e^{-i\gamma(A-D)}$, Eq. (9) becomes

$$|\psi(t)\rangle = e^{-i\gamma At} e^{-i\gamma Dt} |\psi(0)\rangle. \quad (10)$$

The factor $e^{-i\gamma Dt}$ is a global phase and only results in a difference in observed behaviour if the degree of the graph on which the walker evolves is not fixed [31]. In this work only fixed graphs are considered, but in the simulation the degree matrix is still included for completeness. Comparing Eq. (9) to Eq. (3) it is easy to notice the similarities between continuous and coined quantum walks: they both follow unitary evolution, the first with $U = \exp(-iHt)$ and the

second with $U = S \cdot (C \otimes \mathbb{1}_d)$. Reconciling the two, in the continuous-time limit, is not as easy as in the classical case, but work on it has been done by Strauch [32] and Childs [33]. This report, however, only focuses on continuous walks and their dynamics, so the more subtle mathematics will be omitted.

To show how a continuous quantum walk differs from a discrete one, a continuous walk on a line was simulated and the results are shown in Fig. 3. As for most of the simulations that will follow in this report, the value of γ was set to 1 for convenience, as in a fixed graph it is only a scaling constant. The quantum walk was again compared to the classical one, as was their standard deviation. The quantum interference effects give the continuous walk a shape that is

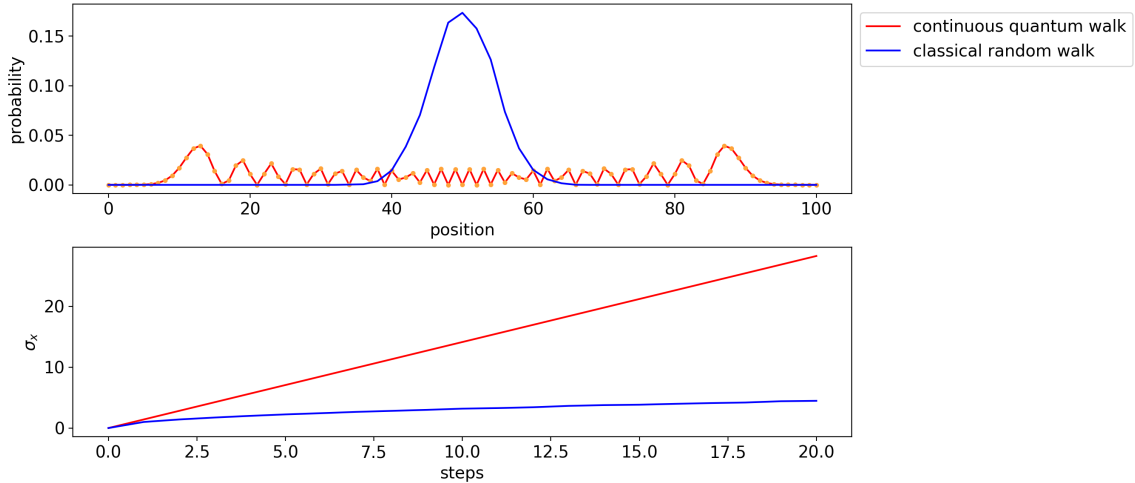


FIG. 3: Continuous quantum walk and classical random walk after 20 steps (top), and standard deviation for both walks (bottom). The classical random walk was averaged over 10000 trials.

similar to that of the coined walk, but with some important differences. Without a coin, there is no initial bias, so the walker evolves symmetrically to the left and right of its starting position. The shape of the distribution is similar, but the peak probability is lower: this is because the continuous walk supports both even and odd sites, whereas the coined one is tied to the parity of the steps it takes. This means that a continuous walk can be found in twice the number of states, and to conserve its normalisation, the peak probability must decrease. Comparing the standard deviation the similarities with the coined walk are again clear: the spreading is linear and therefore faster than the classical one. The continuous quantum walk also appears to be twice as fast as the coined walk, due to the high value of the hopping rate γ . Despite this being a simple simulation it is again a useful proof of concept and sanity check that the model behaves as expected, and can be used in more complex settings.

3. SQUARE LATTICES

The next step is to move to a higher dimension, which reflects a more realistic setting and sets the ground work for section 3, where lattices of more interest will be simulated. This section will investigate the dynamics of quantum entities on a 2-dimensional square lattice, and will explore the consequences of some effects that could be of interest for future works. Thanks

to the relatively simple mathematical framework of continuous quantum walks, moving from 1 to 2 dimensions only requires a modification of the Hamiltonian of the system. This is done by building an adjacency matrix that reflects the geometry of the lattice that is being simulated. A higher dimension necessarily implies a larger matrix, as the size of A is tied to the number of position states, or nodes, on the graph. The definition of A , however remains the same, with its entries $A_{i,j}$ being non-zero when i, j are not connected. The value of γ was again set to 1 for convenience. One interesting consequence of this flexibility in the mathematical formulation is that the lattice can be very easily modified to have reflective edges, or become a torus or a tube. A torus is constructed by setting the value of $A_{n,m}$ to 1 when n is a state in the bottom (or right) edge of the lattice and m is a state in the top (or left) edge. The adjacency matrix for the tube is built in a similar way, but only one side is connected to its opposite. The evolution of a particle on the square lattice is shown as a colorplot in Fig. 4, before having hit the edge of the graph. The particle evolves from the middle and the probability distribution peaks at

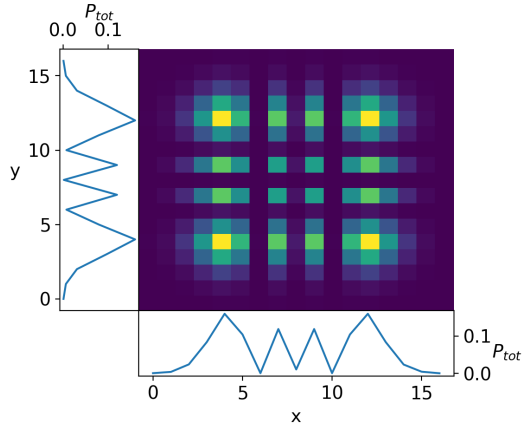


FIG. 4: Probability distribution of a 2D quantum walk after 10 steps. The total probability in each dimension is shown on the sides of the graph.

its four corners. Recovering the probability distribution in 1 dimension, by summing over the probabilities along the y and x axes, the shape from the continuous quantum walk in section 2 is recovered, showing that the particle is spreading in a similar fashion. The symmetry is clearly still conserved, and the walker evolves in all 4 directions in the same way. Once the particle reaches the edges of the graph its behaviour changes depending on the structure of the lattice. As it can be seen in Fig. 5(b), a lattice with reflective edges and one shaped like a torus will induce different reflection and interference patterns in the wavefunction of the walker. The probability distribution, however, remains symmetric and eventually reaches a more stable distribution, as will be shown later in this section.

A. Introducing additional effects

What can break the symmetry of this ideal quantum walk is the addition of a non-symmetrical potential. In a classical setting a high potential can be thought of as a wall, and a low potential as a hole. In quantum mechanics, however, due to interference effects high and low potentials have the same effect on a wavefunction, meaning that a particle will not fall into

a hole, but rather bounce off it. A possible workaround for future works will be mentioned in the form of particle interactions later in this section. To introduce a potential onto the lattice the Hamiltonian H needs to be modified. The diagonal entry $H_{i,i}$ of the Hamiltonian effectively represents the energy of the state at position i , therefore adding a potential is as simple as modifying this entry. The symmetry of the lattice is broken by increasing or lowering the value of $H_{i,i}$, introducing an obstacle in the path of the particle. This can be formalised as:

$$H'_{i,i} = H_{i,i} + p, \quad (11)$$

where p is the value of the potential. The effects of this modification can be seen in Fig. 5, where the evolution of a particle is compared on the same lattice. In Fig. 5(a) the particle has not hit

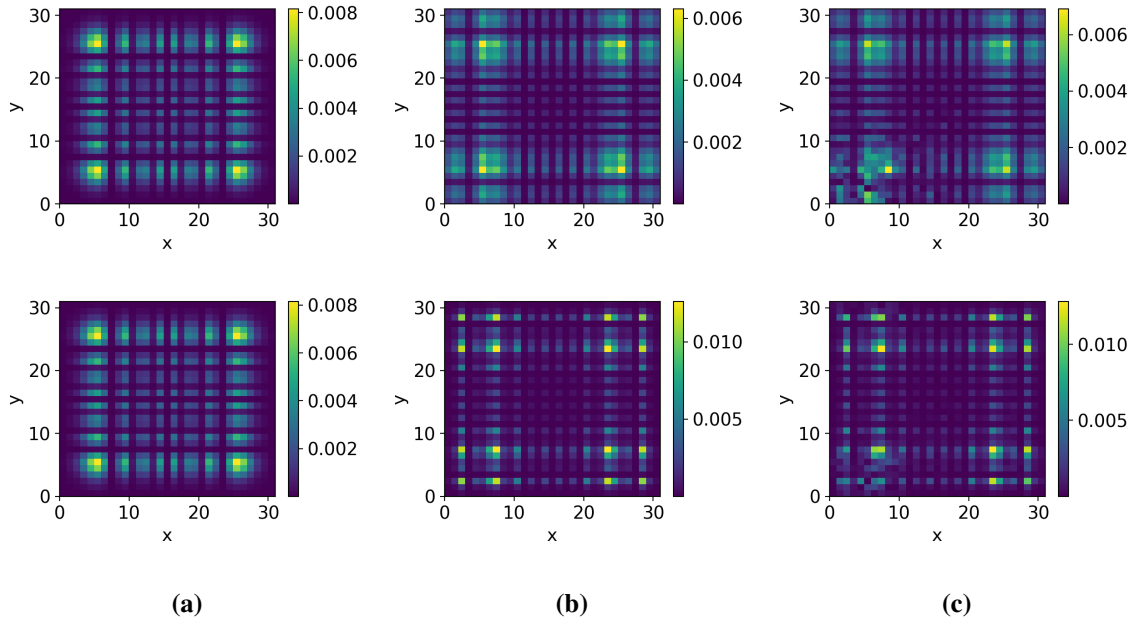


FIG. 5: Evolution of a particle on a lattice after 20 steps (a), 40 steps (b) and 40 steps with a high potential in the bottom left corner (c). Plots show reflective edges (top), and toruses (bottom).

the edges of the lattice yet, and its evolution is identical for the graph with reflective edges and the torus. In Fig. 5(b) there is a noticeable difference in how the particle behaves after hitting the edges, but the symmetry is still conserved and the distribution is relatively stable. In the last case, shown in Fig. 5(c), the effect of the potential added to one state in the bottom left corner shows how the symmetry of the system can be easily broken with a small modification. The simulations that will be shown in the rest of this work will not include asymmetrical potentials of this kind, as they will focus more on ideal cases, trying to build a simpler model of more complicated physics. The potentials described here, however, could be used in future works as a model of simple defects, comparing the dynamics of an asymmetrical lattice to those shown in this report.

Another effect that can disrupt the dynamics of the quantum walk is the interaction with the environment. In a realistic setting the system would not be completely isolated, but

would instead partially couple with the macroscopic environment. This interaction takes the name of decoherence and it is one of the biggest challenges that quantum engineering faces, reducing quantum phenomena to classical behaviours. In this work the focus will remain on ideal condition, without decoherence, not only because it is interesting to study pure quantum effects, but also because simulating decoherence can be very demanding for the hardware that is available. The higher computational demand comes from the need to move from a simple unitary evolution of the wave vector to the density matrix formalism [34]. In this formalism the wave function of the walker is redefined as its density matrix $\rho = |\psi\rangle\langle\psi|$, which evolves as

$$\frac{d\rho(t)}{dt} = -i\gamma[A, \rho], \quad (12)$$

where A is the adjacency matrix. For uncorrelated noise in the $\delta t \rightarrow 0$ limit, Eq. (12) becomes:

$$\frac{d\rho(t)}{dt} = -i\gamma[A, \rho] - p\rho + pP\rho, \quad (13)$$

where p is the decoherence rate, and P represents the effect of random noise, which can be expressed as the set of projectors $\{\mathbb{P}_i\}$ acting on ρ as

$$P\rho = \sum_i \mathbb{P}_i \rho \mathbb{P}_i^\dagger. \quad (14)$$

The extra terms in Eq. (13), compared to Eq. (12), have the effect of shrinking the off diagonal elements of the density matrix. Simulating the effect of decoherence required solving Eq. (13) by numerical integration, which introduced some approximation error into the code. The timesteps were tuned to reduce these inaccuracies, but this still limited the size of the simulation. Despite these inaccuracies, the results shown in Fig. 6 and Fig. 7 still agree with the intuitive prediction that a high decoherence rate p would reproduce classical behaviours. In one dimension the shape of the continuous walk on the line is recovered for $p = 0.0$, and as the rate of decoherence increases the probability distribution slowly reduces to the binomial distribution, observed for $p = 1.0$. At $p \approx 0.04$ the shape of the walk is close to a top hat distribution, which

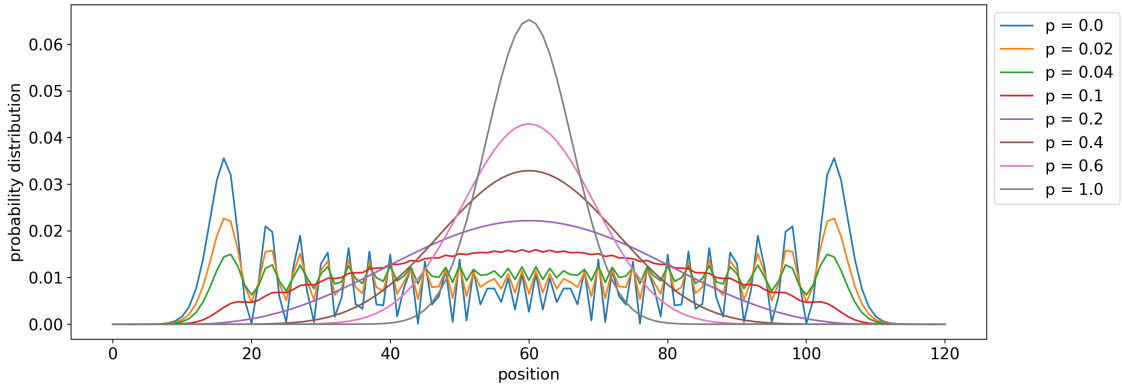


FIG. 6: Probability distribution of a continuous quantum walk on a line after 100 steps, for increasing decoherence rate.

dimension the shape of the continuous walk on the line is recovered for $p = 0.0$, and as the rate of decoherence increases the probability distribution slowly reduces to the binomial distribution, observed for $p = 1.0$. At $p \approx 0.04$ the shape of the walk is close to a top hat distribution, which

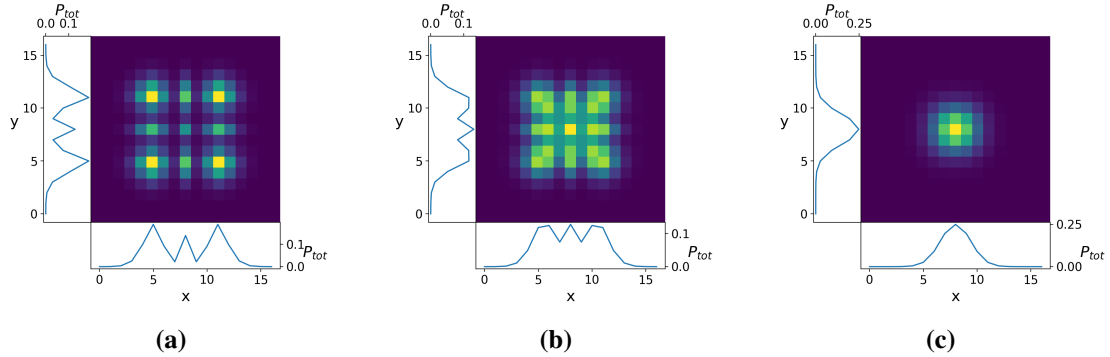


FIG. 7: Probability distribution in 2D (colorplot) and for each dimension (side plots) after 10 steps.

Decoherence rate set to 0.0 (a), 0.2 (b) and 1.0 (c).

is particularly helpful in algorithms where uniform sampling is required. For 2 dimensions the effect of decoherence was made clearer by plotting the probability distribution in both axes. For $p = 0.0$ we recover the result of Fig. 4, as expected, whereas for $p = 1.0$ the distribution is clearly binomial and classical. The role of decoherence is crucial in the engineering required to build a quantum system, but this report tries to build a more ideal framework, therefore the following simulations will be run without decoherence.

One of the tasks a quantum computer would improve is the simulation of quantum systems: a quantum particle will be in a superposition of 2^n states, whereas classical bits scale quadratically as n^2 . This means that simulating complicated quantum systems on a classical computer is incredibly resource heavy. This becomes apparent very quickly, even when trying to simulate two particles. Introducing a second particle also gives the opportunity to model and observe the effects of attraction and repulsion between the two. In these simulations the particles were modelled as hardcore bosons, meaning they could not occupy the same state but could exchange position without inducing a phase shift in their wave functions. The Hamiltonian of this new system was created by taking the tensor product of the adjacency matrices of the two particles, giving $A_{2 \text{ particles}} \equiv A' = A_{\text{particle 1}} \otimes A_{\text{particle 2}}$. Because the particles cannot occupy the same position, the rows and columns corresponding to these forbidden states were removed from A' . This means that the "hardcore" part of the hardcore boson was hard coded into the simulation. The exchange symmetry, however, was a result of unitary evolution, and had to be verified. This was done by initialising the two particles in entangled states $|m\rangle|n\rangle - |n\rangle|m\rangle$ and $|n\rangle|m\rangle - |m\rangle|n\rangle$ and comparing their evolution. After the same number of steps they were found to be in the same state, therefore proving that they are symmetric. Adding a second particle by taking the tensor product of the two adjacency matrices does not introduce any additional interaction, therefore to add effects such as attraction and repulsion some entries of A' must be modified. Every state i in this new adjacency matrix describes the position of both particles and thus has a cartesian distance L_i associated with it. The way inter-particle interactions were implemented was by setting a distance threshold T : if $L_i - L_j > T$, then $A'_{i,j}$ is lowered in the case of attraction and raised in the case of repulsion. This means that the two particles that repel (attract) each other have a higher (lower) probability to go between two states that increase their distance. In the simulations more than one threshold was defined, in order to make the levels of interaction more granular. The results of the first simulations on

a square lattice can be seen in Fig. 8, where the effects of the interactions are shown after 20 steps. The two particles were initialised at a distance of $\sqrt{2}$ and left to evolve on a relatively

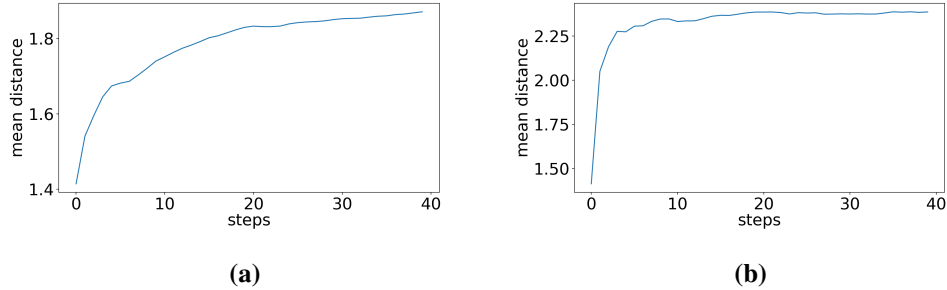


FIG. 8: Square lattice of side 6. Running average of the mean distance for two attractive (a) and repulsive (b) hardcore bosons.

small lattice. The average distance soon reaches a maximum value due to the particles reflecting off the edges, but a difference is clearly observed between attraction and interaction, with the attractive particles being almost a third closer than the repulsive ones. To make the effect more drastic and obvious the shape of the lattice was changed. This required a simple modification of the adjacency matrix for each particle, fitting them to the new geometry of the lattice. The extreme case is shown in Fig. 9, where the two particles evolve on a line, and are initialised at the opposite edges of the graph. The effects of inter-particle interactions are even more pronounced,

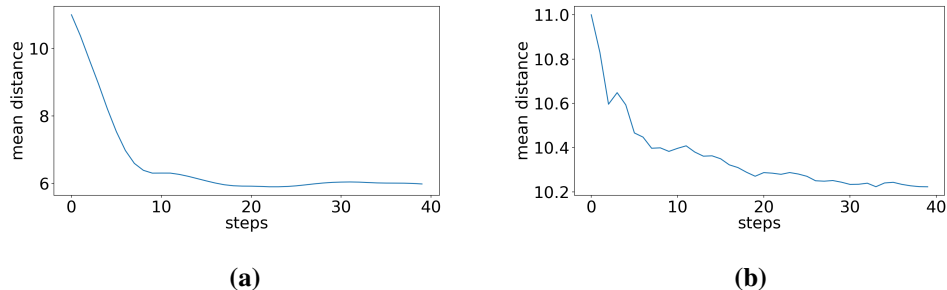


FIG. 9: Evolution on a line of length 15. Running average of the mean distance for two attractive (a) and repulsive (b) hardcore bosons.

with the attractive particles moving much closer than the repulsive ones, thus proving that this model of attraction works in the way it was predicted. The focus of this report will remain on the dynamics of a single particle, but for future works this form of interaction could be a useful alternative to potential gradients, since the quantum effect of a low potential is to effectively turn a gradient into a trough.

B. Measuring transport properties

The standard deviation was used in section 2 to study the transport properties of continuous quantum walks on the line. Similarly, for a walk in 2 dimensions, the radial standard deviation σ_r was defined and plotted against time, to study how the particle spreads in the square lattice.

Using the tools developed to reshape the graph, the radial spread was plotted for lattices of different width, going from a square shape to a more narrow geometry. As shown in Fig. 10,

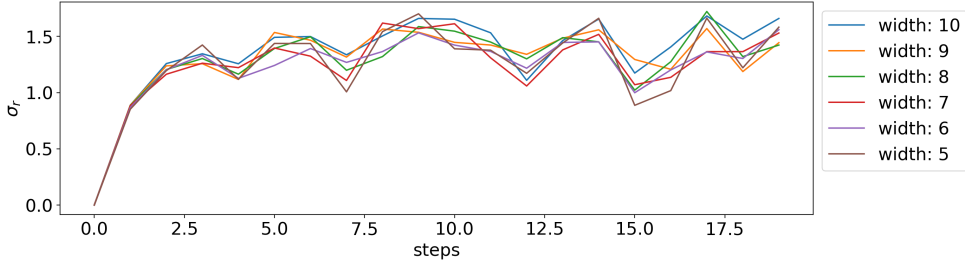


FIG. 10: Radial standard deviation on a square graph of length 10 and variable width.

the initial behaviour of the system is the same regardless of the shape of the graph: the standard deviation grows linearly, as in the case of the walk on the line, but less rapidly, probably due to the added degree of freedom. The walk then reaches a maximum value for σ_r and oscillates around it. This maximum value is hit when the walk reaches the edges of the lattice and starts reflecting back. It is lower for narrower graphs, but the difference is not drastic, and the overall behaviour remains very similar. The radial spread, however, is not the only measure of the dynamics of quantum walk that will be used. Another important quantity is the arrival probability, defined as the sum of the probability that has reached a certain part of the lattice. This measurement is particularly useful in lattices that are narrower than a square lattice, and have a geometry more similar to that of a tube, as will become clear in the next section. Here an example of how this quantity can give a useful insight is shown for a square lattice, where the size of the graph is reduced in the vertical direction. To record the probability that arrives at the desired sites a quantum sink is set up, using a simple model of loss. This sink is usually located on the right of the graph, and the particle is initialised in a superposition of the states on the left. Once the wave function reaches the right side of the lattice its probability leaves the system, and it is recorded as arrival probability. This is done by adding an imaginary term to the Hamiltonian. For a sink in position j :

$$H_{j,j} = H_{j,j} - i\frac{\eta}{2}, \quad (15)$$

where η is the loss rate. This quantity gives a good measure of how quickly the particle reaches the opposite side of a long and thin lattice, and will be used extensively in the next sections. Fig. 11 shows a simple example of the arrival probability in a square lattice. Because of the high symmetry of this setup, the walk in Fig. 11 evolves much like a walk on a line, since the initial state was a superposition of all the nodes on the left. Regardless of the width of this square tube, the arrival probability and horizontal standard deviation evolve in the same way, confirming the high degree of symmetry of this system. The horizontal spreading begins to oscillate once the particle reaches the opposite edge of the graph. The arrival probability climbs relatively quickly once the sink sites on the right are reached, and then asymptotes to a value less than 1 for the long term limit. This is a very interesting and purely quantum effect: if a classical walk has a sink, the walker will eventually and inevitably fall into it, but for a quantum walk, some of the eigenfunctions of the particle might not have any support on the states where the sinks are and

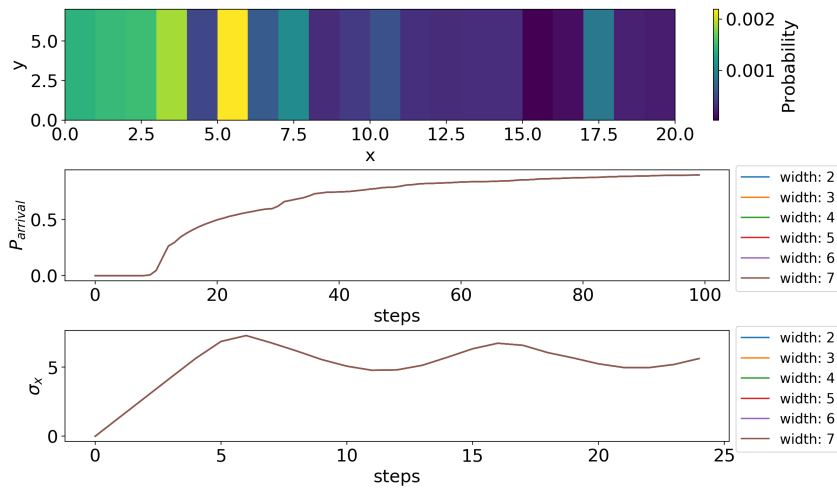


FIG. 11: Arrival probability and horizontal standard deviation for a square graph of variable width. The colorplot shows the probability distribution after 100 steps, when sinks were set up on the right edge of the graph.

will therefore remain on the lattice. These eigenfunctions correspond the real eigenvalues of the Hamiltonian, since the sink was introduced as an imaginary term. In some cases the arrival probability will not reach unity, and some probability will remain on the lattice.

Now that the mathematical tools have been built, and the most useful measures of the transport properties have been tested on a simple square lattice, some more interesting graphs will be examined, such as the hexagonal ones in the next section. The geometry of hexagonal lattices is particularly interesting because it can be compared to physical structures such as graphene and, when modified in a similar fashion to Fig. 11, carbon nanotubes.

4. HEXAGONAL LATTICES

Graphene has been the subject of much interest since it was first produced and identified in 2004 by Novoselov *et al.* [35], due to its unique electrical [36] and mechanical [37] properties. An algorithm for quantum search using continuous quantum walks has recently been implemented by Foulger [20]. In this work the continuous quantum walks will be applied to different types of hexagonal lattices to study their transport properties. A similar study was conducted in [38] using coined quantum walks. Discrete and continuous walks generally give similar results for the same graph, so the results from [38] will be compared, at least qualitatively, to the findings of this report. To build a hexagonal lattice on which the simulation will be run, the python library *networkx* was used, as it provides very useful tools to build various types of graphs and easily obtain their properties, such as their adjacency matrix. It is important to know that due to the way *networkx* assigns coordinates to the nodes of the graph, for the hexagonal lattice each hexagon is one unit in length and two units in height. This will become apparent in the following examples, especially where the vertical and horizontal spreads will be analysed. This will not constitute a problem, as the number of hexagons will remain the same, but particular

care will need to be taken when comparing results. A hexagonal lattice breaks some of the symmetry compared to the graphs in section 2. Each node, except those at the edges of the graph,

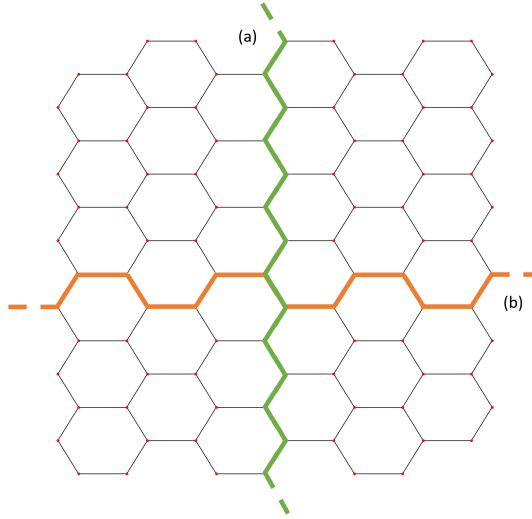


FIG. 12: Hexagonal lattice with trajectories a particle would follow on an armchair (a) and a zig-zag structure (b).

has degree 3, and the lattice has a rotational symmetry of π . This means that the dynamics in perpendicular directions will be different. As shown in Fig. 12, if the particle moves with trajectory (a) it follows a more direct path than (b). This will lead to differences in the transport properties of a particle moving in different directions.

Before more advanced graphs are studied, a simple 2-dimensional lattice is simulated, as a useful comparison for the dynamics of a particle on a hexagonal lattice. The particle is ini-

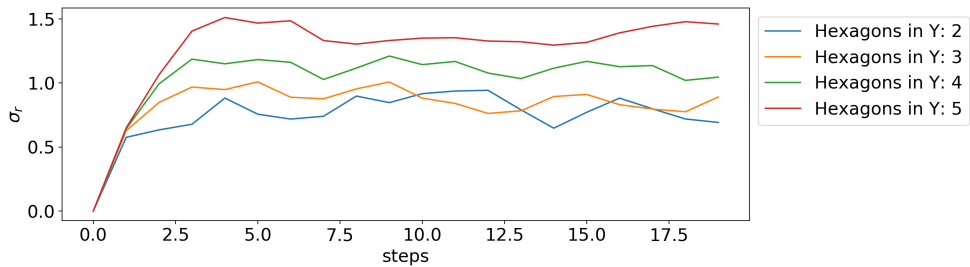


FIG. 13: Radial standard deviation for a particle on a hexagonal lattice of length 6 and variable width.

tialised in the middle of a lattice with reflective edges and left to evolve. The radial standard deviation was recorded in a similar fashion to Fig. 10, measuring the cartesian distance from the starting position. Fig. 13 shows the radial spreading for a hexagonal lattice with varying vertical dimension. The standard deviation grows linearly until it hits the edges of the graph, and then remains roughly constant at a value proportional to its height. This behaviour is similar to that observed in the lattices studied in section 2. For the hexagon, however, the walker spreads much more slowly, as can be seen from the gradient of the initial linear spread, which is approximately half of that seen for a square lattice. Reducing the symmetry of the underlying graph therefore has a clear and important impact on the dynamics of a continuous quantum walk, reducing its mobility.

A. Carbon nanotubes

Dynamics on graphene sheets are useful to set up a model for hexagonal lattices, but most physical implementations of this material come in the form of carbon nanotubes. These structures, built by wrapping a sheet of graphene onto itself, are a great engineering challenge, but offer the same mechanical advantages as graphene. Unlike graphene, which has the electrical properties of a semimetal, carbon nanotubes behave like semiconductors or metals depending on the way they are constructed [40]. A detailed description of the geometry of carbon nanotubes can be found in [39], but in this work only the fundamentals will be outlined. Because they are closely related to graphene, carbon nanotubes are described in terms of graphene lattice vectors. Their structure is characterised by their circumferential vector, defined as

$$C_h = n\mathbf{a}_1 + m\mathbf{a}_2, \quad (16)$$

where \mathbf{a}_1 and \mathbf{a}_2 are the graphene lattice vectors, and n, m are the relative positions of the atoms that are connected when the graphene sheet is rolled into a tube. Nanotubes with $m = 0$ are defined as zig-zag nanotubes, and nanotubes with $n = m$ are defined as armchair nanotubes. Practically, if the graphene sheet in Fig. 12 is made into a nanotube by connecting its top and bottom edges, its structure becomes a zig-zag nanotube. If the left and right edges are connected, it becomes an armchair nanotube. Their 3-dimensional geometry is shown in Fig. 14. To simulate the transport properties on a carbon nanotube the particle is initialised in a

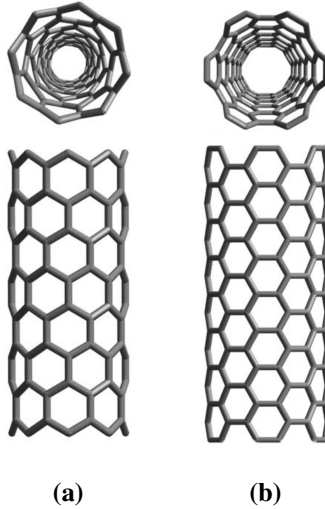


FIG. 14: Three dimensional structure of zig-zag (a) and armchair (b) carbon nanotubes, with top and side view.

superposition of the states at the bottom of the tube. Unlike the case for the square lattice, this state is not perfectly symmetrical and will therefore not continue to be in a perfect superposition of all the states on the horizontal dimension. Theoretical results predict a faster transport on armchair nanotubes, as these exhibit metal behaviours, whereas zig-zag nanotubes behave as semiconductors [40]. To construct a graph that would behave like a nanotube a hexagonal lattice

similar to Fig. 12 was created, with the number of hexagons in one dimension being larger than the other. The long sides were then connected by modifying the entries of the adjacency matrix, meaning that in the graphs showing the results, the tubes will be displayed as flat. The quantities that were measured are: the standard deviation along the dimension with the greater number of hexagons, the arrival probability, as defined in the previous section, and the average position of the particle, defined as the 1-dimensional distance from the starting position. These are plotted against time to show how fast a particle spreads in a nanotube structure. The first examples are of simple zig-zag and armchair nanotubes of fixed length and width.

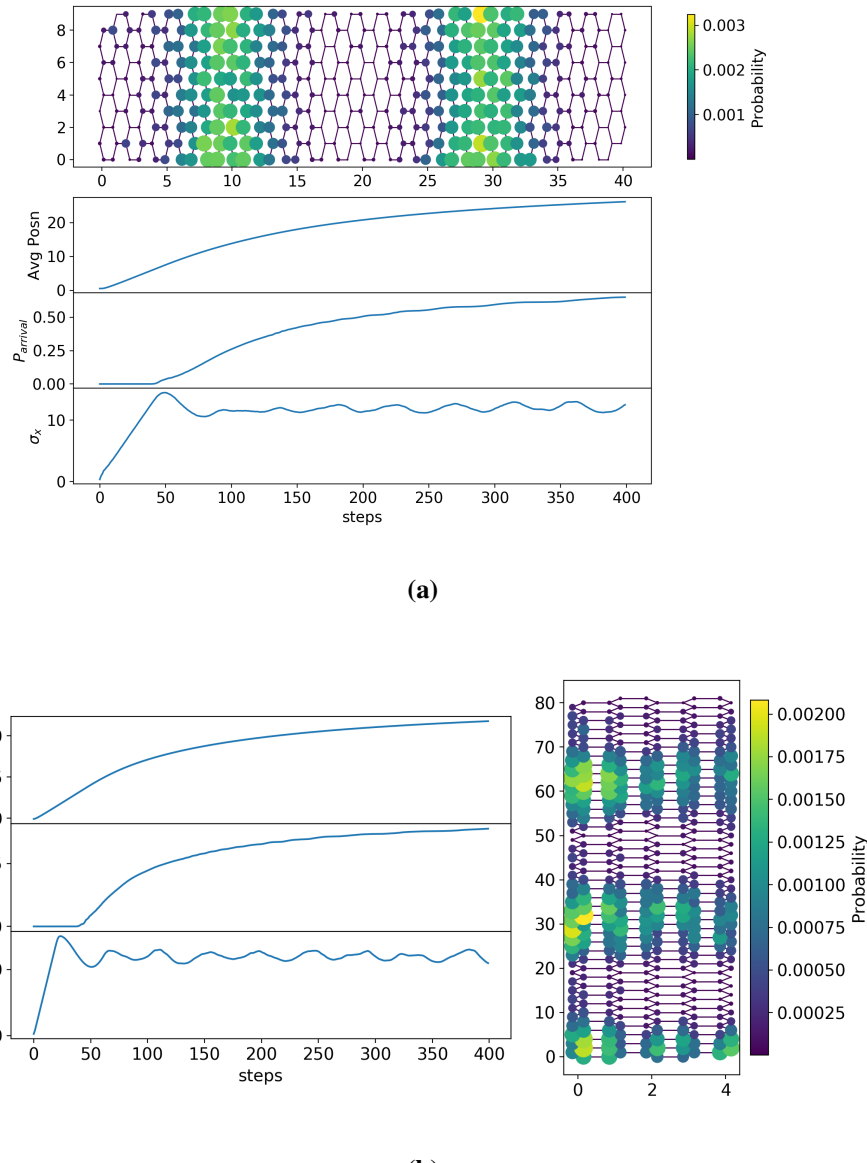


FIG. 15: Transport properties of a zig-zag (a) and armchair (b) nanotube of length 40 and width 4. The size and colour of the nodes is proportional to the particle probability. The colorplot shows the particle after 400 steps when sinks were set up at the right (a) and top (b) of the tube. Both tubes are 40 hexagons long and 4 wide.

Fig. 15 (a) and (b) show the results from the first simulations of the carbon nanotube structures, alongside the measures of their transport properties. As mentioned before *networkx* plots the hexagon to be 1 unit wide and 2 units tall, therefore this will need to be taken into consideration when comparing the standard deviation and the average position. The hexagonal graphs show the particle at the end of its evolution, when sinks have been set up in the end sites of the tube, in order to record the arrival probability. The leftover probability shows some clear oscillations, which can be interpreted as the eigenfunctions that remain onto the graph as they have no support over the states where the sinks are. Some of the eigenvalues of the Hamiltonian of this system, in fact, are real, confirming that part of the wavefunction of the particle will remain on the lattice. This can also be observed from the fact that the arrival probability asymptotes to a value less than one, again suggesting that some eigenfunctions will continue to oscillate on the graph, never reaching the sinks. Comparing the dynamics of the two different structures, the armchair nanotube approaches a higher arrival probability faster, meaning that the particle moves more quickly towards the opposite side of the tube. This result is consistent with intuition, since the particle has a more direct path when compared to the zig-zag structure. Similarly, the standard deviation shows the armchair nanotube spreading more rapidly, despite both structures exhibiting a similarly linear behaviour until a stable value for σ is reached. The average position rises slightly faster for the armchair nanotube, and settles to a value of about three quarters the length of the tube for both structures. As previously mentioned, theoretical results predict zig-zag nanotubes to behave like semiconductors, while armchair ones exhibit metallic characteristics. The results of these simulations concur with these predictions, despite not accounting for the different conduction models, proving that this simple model of transport properties can give useful insight into the dynamics of particles on fixed graphs. The work done in [39], using coined quantum walks, reached the opposite conclusions, suggesting that continuous quantum walks are a better model for these types of graphs.

The general description of a carbon nanotube was presented in Eq. (16), but so far only the special cases of a zig-zag and armchair structure have been presented, which take the name of achiral tubes. In the case where $m \neq 0$ and $m \neq n$, the nanotube becomes chiral [40], and loses some of its symmetry. Practically this is achieved by connecting the graphene lattice in a similar way to the zig-zag tube, but shifting one side $n - m$ units up. A lower chiral shift will result in a structure closer to the zig-zag nanotube, whereas a higher one will be more similar to an armchair structure. This different geometry will cause the direct path from one end of the tube to the other to become a combination of the armchair and zigzag one, as shown in Fig. 16. To study the dynamics of the chiral nanotube a comparison needs to be drawn to the achiral structures. The arrival probability is a good description of how a particle spreads from one end of the nanotube to the other, as seen in previous examples, and can therefore be used as a means of comparison. The number of steps taken to reach an arrival probability of 50% was plotted against the dimension of the tube for the three different structures. Fig. 17 (a) shows that for longer nanotubes of the same width more steps are needed to reach the opposite side, and that different geometries exhibit different behaviours. Previous results are confirmed, showing that a zig-zag nanotube always takes more steps to reach the same arrival probability, when compared to the armchair structure, for the same width and length. As expected, the chiral nanotube behaves like a combination of the two structures, with the number of steps always being between those of the achiral graphs. A more surprising result comes from Fig. 17 (b),

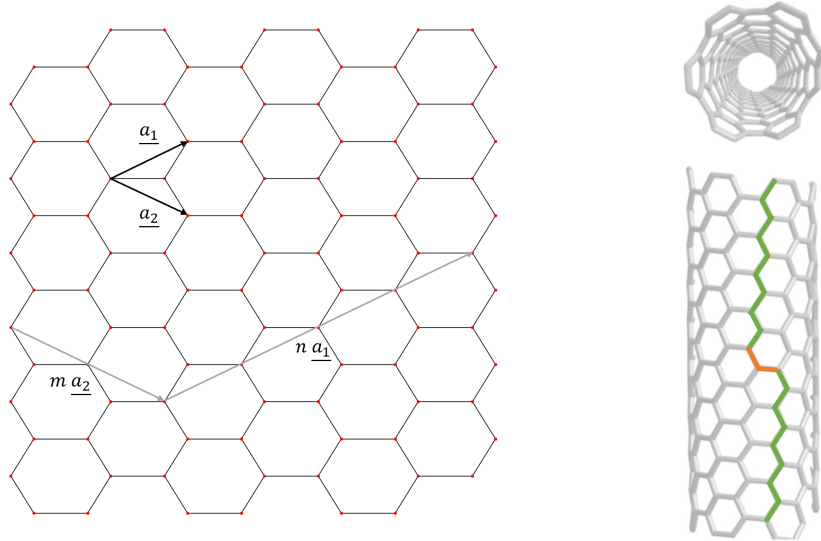


FIG. 16: Lattice vectors and components of the circumferential vector for a chiral nanotube on the left, three dimensional structure of a chiral nanotube on the right, with the most direct path shown as a combination of armchair (green) and zig-zag (orange) structure paths.

where the number of steps to reach 50% arrival probability is plotted for different widths at the same length. Here the behaviour of the achiral nanotubes is roughly constant, since the particle was initiated in a superposition of all the states at one end on the tube, and the armchair structure consistently outperforms the zig-zag one. The chiral nanotube, however, seems to behave like an armchair structure at smaller widths, and like a zig-zag one at higher widths. The unexpected results at low widths suggest that the particle might be moving in a path more similar to that of the armchair nanotube, due to the extreme distortion caused by the very low width. It is important to notice that the engineering challenges behind the fabrication of such structures

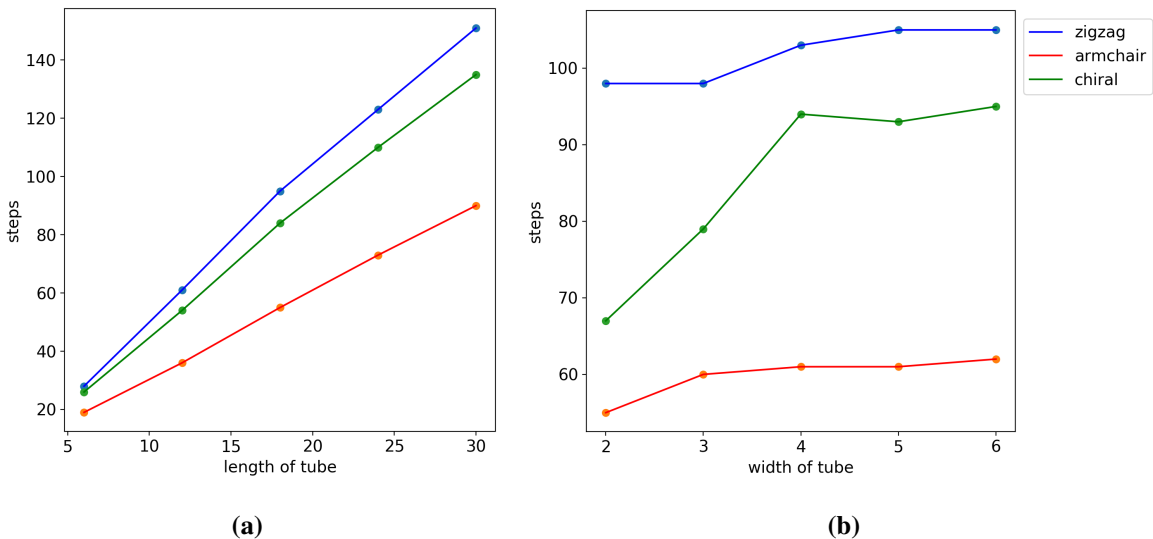


FIG. 17: Number of steps to reach 50% arrival probability for a tube of width 4 and variable length (a) and a tube of length 20 and variable width (b) for chiral and achiral structures.

mean that such low widths will probably not be achieved, and the more relevant results are those that more closely correspond to previous predictions and intuition.

Continuous quantum walks have proved to be a successful model of the dynamics of simple particles on nanotubes, confirming the transport properties of different structures despite not directly accounting for their electrical properties. This proves that a relatively simple theoretical framework can give useful insights into the physical behaviour of these and similar structures. The aim of the next section is to explore the transport properties of graphs with a higher degree of randomness, employing the same tools that have been successfully used in this section.

5. CLUSTER LATTICES

Moving from an ideal case of very high symmetry in the square lattice, to one where the symmetry is only partially broken in the hexagonal graph, caused a noticeable effect to the transport properties of the continuous random walk. A lower symmetry reduced the speed of the spreading and caused the arrival probability to rise more slowly. A hexagonal lattice, however, still represents an ideal case of relatively high symmetry. It is reasonable to assume that a more random lattice would amplify these effects, slowing down the particle even more. The graphs studied in this section were built to resemble structures similar, at least conceptually, to domains such as those found in magnetic materials. These structures are characterised by clusters of nodes that have a high degree of connectivity and varying degrees of symmetry. The connections between clusters vary according to the dimension of the material: on a plane, only clusters that are next to each other can be connected, whereas in a three-dimensional structure each cluster can be connected to any other. In this work the first case will be referred to as next-cluster connections and the second as random connections. The clusters in this section will be arranged next to each other in a line, as this structure more closely resembles that of the nanotubes studied in section 4, and will make comparisons more clear.

A. Random clusters

The first simulations will be run on clusters that have no regular structures. Each cluster has the same number of nodes, located in random positions within the bounds of the cluster, and randomly connected between each other, as shown in Fig. 18. Each cluster is 10 units long in the horizontal direction, which is the only direction where the standard deviation will be measured, and the distance between clusters was set to 0 (this is shown as greater in Fig. 18 and Fig. 19 for clarity). This high degree of randomness implies that the particle has no

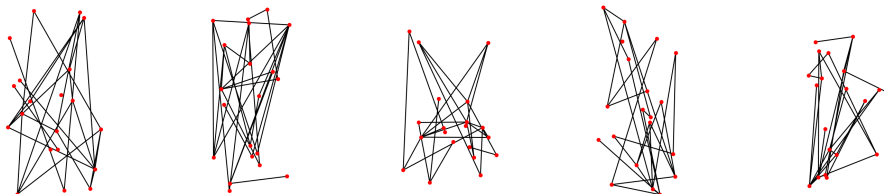


FIG. 18: Example of a graph made of random clusters, with no connections between the clusters.

clear path to follow, unlike in the examples of a square or hexagonal lattice. The effects of this structure will be studied by measuring the spreading of the particle much like in the previous sections. The clusters can be connected by next-cluster edges or random edges, as shown in Fig. 19. Random edges can be interpreted as highly connected, three-dimensional structures, that

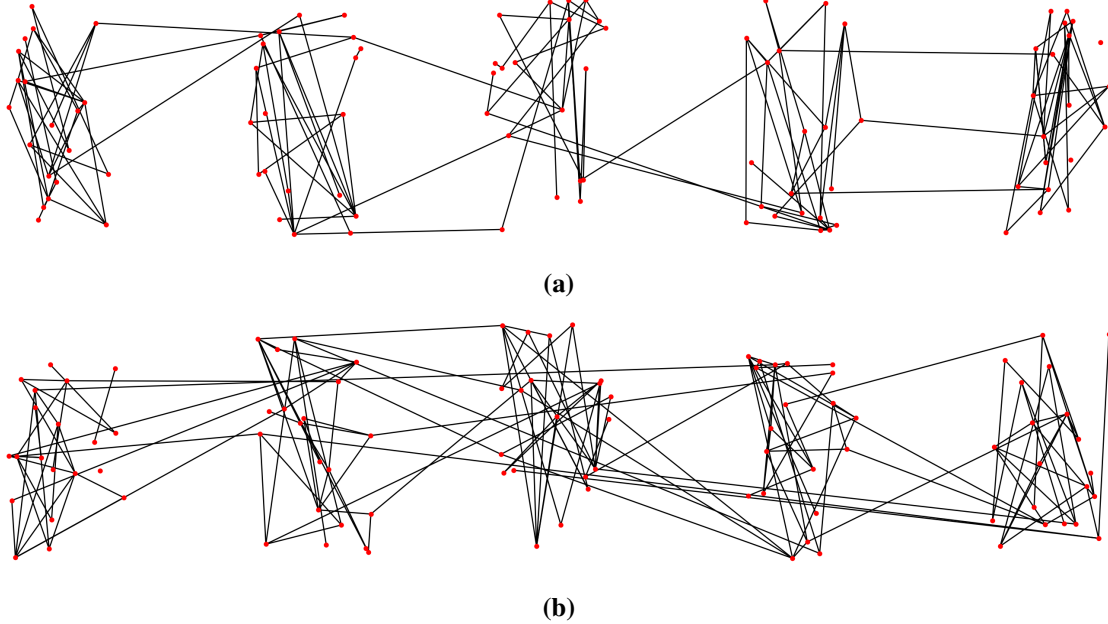


FIG. 19: Graph of random clusters connected by next-cluster edges (a) or random edges (b).

are more evenly distributed in space, whereas graphs connected only by next-cluster edges are more ordered and confined to a lower dimension. This drastically affects the spreading, as can be seen in Fig. 20. In this example the number of clusters was kept the same, and the number of nodes in each cluster was varied, keeping the the number of edges per node in the cluster

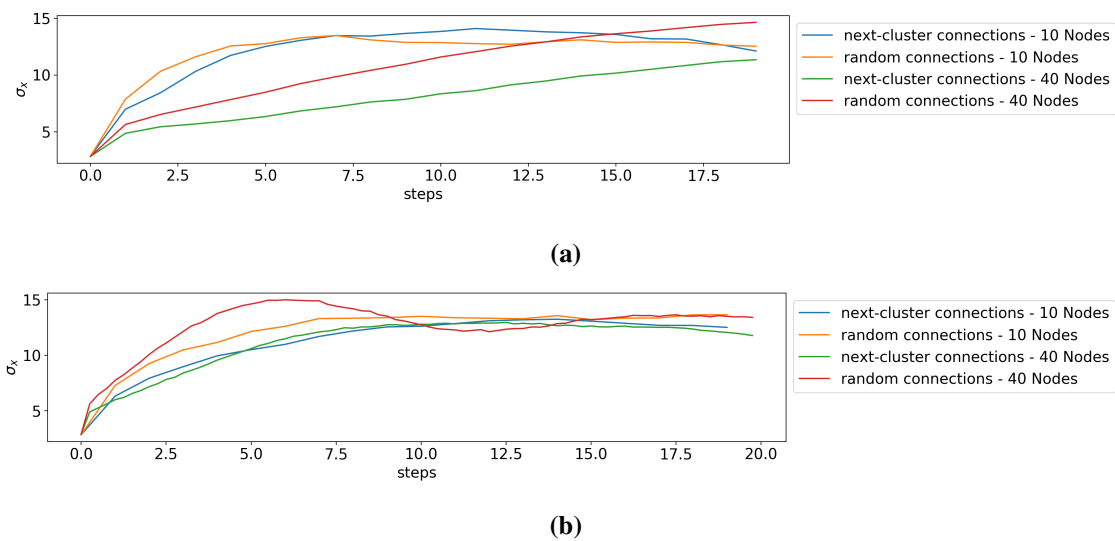


FIG. 20: Horizontal standard deviation for a cluster graph with variable number of nodes (a), also shown rescaled by the ratio of number of nodes (b).

to 2. The standard deviation was calculated for both next-cluster and random connections, fixing the number of inter-cluster connection to be 15 for every case. The quantum walker was initialised in a superposition of all the nodes in the central cluster, therefore the value of its standard deviation starts at a value greater than 0. The graph with random connections clearly and predictably spreads much faster and quickly reaches a stable value, whereas the other graphs struggle to escape the randomness of the cluster. The lattices with more nodes per cluster are also showing a slower spread, since the particle spends more time in the same cluster before leaving it. Rescaling the values of σ_x by the number of nodes in each cluster, as shown in Fig. 20 (b), reveals that the spreading for next-cluster connections is directly proportional to the size of the cluster. The shape of the standard deviation for random connections, instead, is not recovered by the simple rescaling, showing that fewer nodes increase the spread at a rate lower than linear. This shows how random connections lead to faster and more efficient transport in a structure with low symmetry even with large clusters, and how they are less dependent on the number of nodes per cluster. When compared to a regular square lattice, the growth of σ_x is slower than linear for next-cluster connections, but the high connectivity of the random graph make it more efficient for transport. A similar study can be conducted on the same graph by varying the number of connections between the clusters, and keeping the number of nodes constant at 10 per cluster.

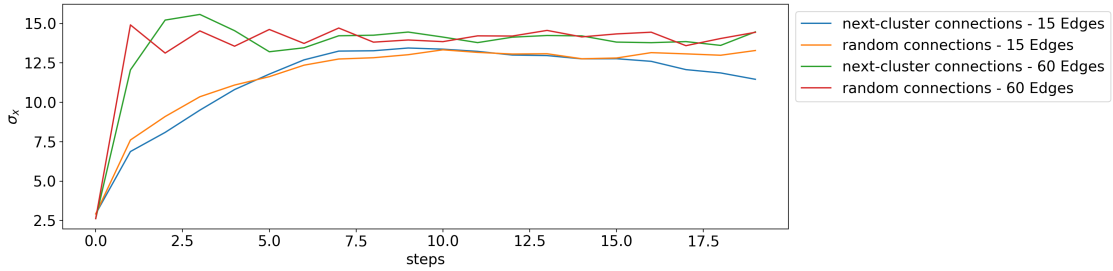


FIG. 21: Horizontal standard deviation for a cluster graph with variable number of edges.

Fig. 21 highlights the importance of connectivity in random walks, as a higher number of edges always outperforms its less connected counterpart, and random and next-cluster connections give very similar results for the same number of edges. Highly connected graphs climb to their maximum value of σ_x very quickly, while less connected ones spread more slowly. Comparing this case to the square lattice we see that the more regular graph is only surpassed by a very high number of connections, which allow the quantum walker to quickly escape the cluster. This is due to the fact that more nodes inside the cluster are connected to other parts of the graph, giving the particle more paths to spread further.

One of the more useful quantities to characterise the transport properties of a quantum walker on a tube was found to be the arrival probability. In section 4 the particle was initialised at one end of the tube and its behaviour at the opposite end was recorded. In this section it is defined in a similar way, with the particle starting in a superposition of all the nodes in the cluster on the left, and sinks set up in the nodes of the cluster at the opposite end. To make a useful comparison to carbon nanotubes the structure of the cluster graph needs to be similar. If a nanotube l hexagons long and w hexagons wide is considered, the cluster structure needs to be built with the same number of total nodes and connections. To do so each cluster has as many nodes as

a w hexagons, and the graph has $l/2$ clusters. The other half of the hexagons are accounted for in the connections between clusters, as w edges are added between each cluster. This is the equivalent of a highly randomised carbon nanotube, and it will highlight the importance of symmetry in the transport of quantum particles. Due to the fact that the connections do not follow a regular pattern, there is no need to modify the adjacency matrix to connect the opposite sides of the graph, as these are likely to be connected already by a random edge. In Fig. 17 the number of steps required to reach a threshold probability was plotted for carbon nanotubes of different length and width. The arrival probability was calculated in the same way, and was plotted after each step for a random graph with a variable number of clusters or cluster nodes. The results shown in Fig. 22 clearly show the disadvantages of random clusters: only for a low

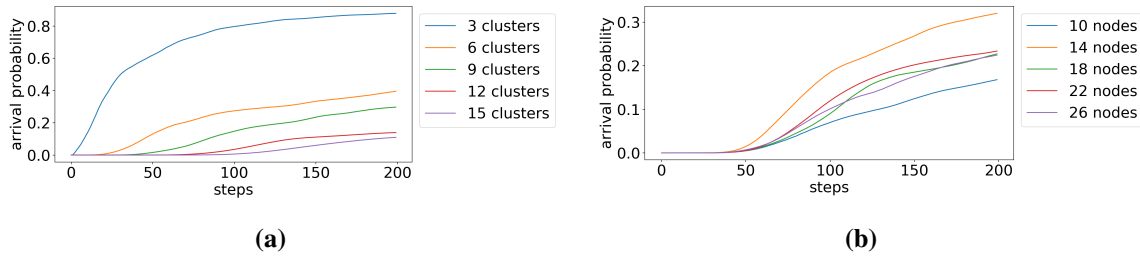


FIG. 22: Arrival probability for cluster graph with next-cluster connections shown for a variable number of clusters with 18 nodes per cluster (a) and variable number of cluster nodes for 10 clusters (b).

number of clusters the particle reaches the threshold arrival probability of 50%. For a graph of fixed length the behaviour is more uniform and random for different widths, but the particle still does not reach the threshold probability, reiterating the importance of symmetry for quantum walks. It was previously shown that random edges can improve the spreading of the particle, therefore next-cluster connections were replaced with random ones, and the arrival probability was recorded again, similarly to Fig. 22. The improvement is noticeable, but Fig. 23 (a) shows

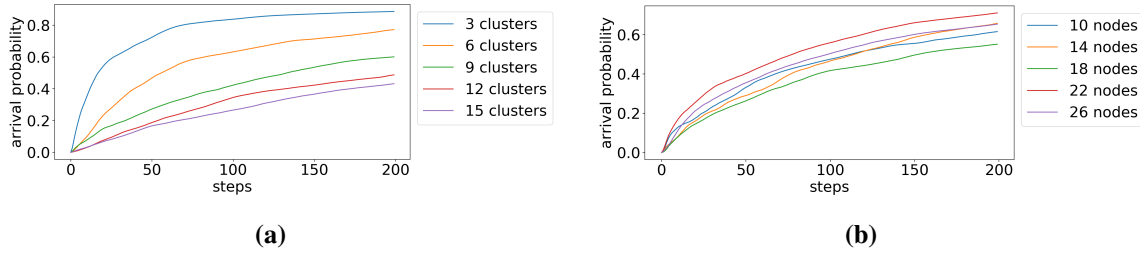


FIG. 23: Arrival probability for cluster graph with random cluster connections shown for a variable number of clusters with 18 nodes per cluster (a) and variable number of cluster nodes for 10 clusters (b).

that for a high number of clusters the arrival probability still cannot reach 50%, even after 200 steps, proving that the more symmetric carbon nanotube provides a more efficient transport. For a varying number of cluster nodes, equivalent to tubes of increasing diameter, the behaviour of the walker is even more uniform than in Fig. 22 (b), and the threshold probability is reached after roughly 100 steps for every width. This is the same number of steps required by the zig-zag nanotube: the least efficient carbon nanotube has the same transport efficiency as the most highly connected random structure.

B. Hexagonal clusters

On a microscopic level structures in nature tend to have some symmetry. Considering, for example, magnetic domains, some resemblance to the graphs analysed above can be seen, but the structure of each domain is more ordered. There is therefore a middle ground between the perfectly regular structures of section 4 and the completely random graphs studied in this section so far. Taking inspiration from magnetic domains, the symmetry is reintroduced within the clusters, while the connections between them are kept relatively random. The most interesting structure that has been studied so far has been the hexagonal lattice, therefore the geometry of the clusters has been chosen to replicate that of carbon nanotubes. Each cluster is composed of a row of hexagons, much like the circumference of a nanotube. In this way the length of this structure can be compared to that of a carbon nanotube in the same way that random clusters were compared to it, while its width is defined by the number of hexagons in each cluster. Despite the random nature of the connections between clusters, the orientation of the hexagons was still considered important and both clusters of zig-zag and armchair structures were simulated. As in Fig. 19, the hexagonal clusters can be connected by random edges, or next-cluster edges, but because they have a more regular structure, a new type of connection can be defined, that is more similar to the connections in carbon nanotubes. This will be referred to as cluster-edge connection and, as the name suggests, it only connects one edge of the cluster to the next, rather than any point in one cluster to any point in the next. Cluster-edge connections are the closest to nanotubes connections, while still conserving some degree of randomness.

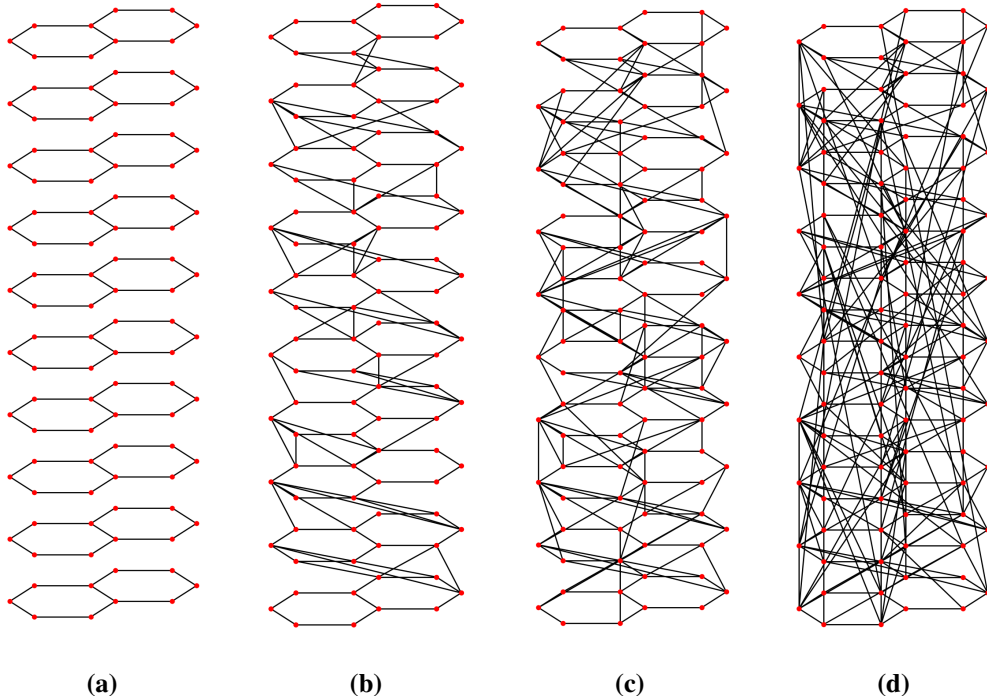


FIG. 24: Hexagonal clusters with no inter-cluster connections (a), cluster-edge connections (b), next-cluster connections (c) and random connections (d).

The geometries in Fig. 24 can be interpreted as a random arrangement of domains in 3 dimensions for (d), a vertical stack of domains for (c) and a 2 dimensional arrangement in a line for

(b). The transport properties of all three geometries were investigated by plotting the arrival probability and standard deviation for each step. The particle was initialised in a superposition of all the nodes in the bottom cluster and the sinks were set up in the top one. As in section 4, when comparing σ for armchair and zig-zag structures, it is important to remember that *networkx* plots hexagons to be 2 units tall and 1 unit wide, so for the armchair structure the value of distance will have to be halved.

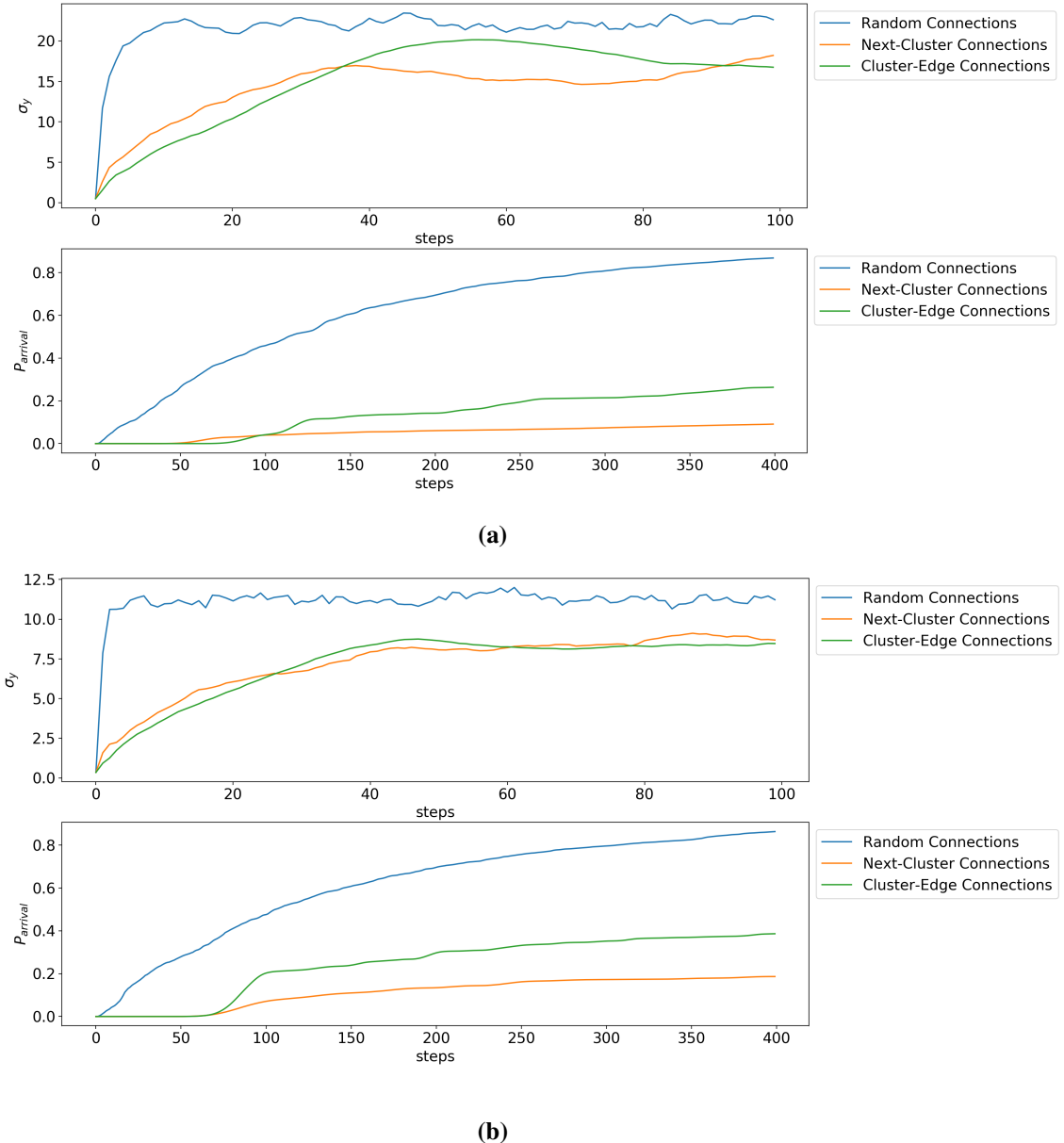


FIG. 25: One dimensional standard deviation and arrival probability for armchair (a) and zig-zag (b) cluster graphs, with 20 clusters and 4 hexagon per cluster.

Fig. 25 (a) and (b) compare different types of connections for the same graph. The standard deviation has a similar behaviour for both cluster structures, rising very rapidly for random connections and settling more gradually to a lower value for next-cluster and cluster-edge connections. The results for the arrival probability are also very similar, where the next-cluster and cluster-edge connections reach a value between 0.2 and 0.3 after 400 steps. The cluster-edge

connections seem to outperform the next-cluster connections slightly, possibly because they more closely replicate the behaviour of more regular nanotubes. Neither of these structures, however, come close to the transport efficiency of graphene. The random connections climb to an arrival probability of 0.8, reaching the arbitrary threshold of 0.5 after around 100 steps. This behaviour is very similar to that of random clusters, for all kinds of connections, suggesting that introducing symmetry in the clusters only has a negligible effect, and that efficient transport of continuous quantum walks requires a high degree of symmetry in the underlying graph.

6. CONCLUSIONS

This work investigated the transport properties of quantum walks, focusing on the standard deviation and arrival probability of continuous quantum walks on different fixed graphs. A theoretical framework for different lattices has been built, starting from a walk on the line and moving to more complex structures in two dimensions. Initially a simple square lattice has been considered, and the effect of added potentials, decoherence and the interaction between two particles have been described. The tools developed on the square lattice were used in the more physically interesting example of graphene and carbon nanotubes, where the armchair, zig-zag and chiral structure were simulated. The armchair structure was found to be the most efficient for transport, proving that this relatively simple model was able to replicate the theoretically predicted transport properties of carbon nanotubes, despite not directly accounting for their electrical properties. More irregular graphs were studied, including completely random structures and more regular cluster graphs. These simulations confirmed that the higher degree of connectivity found in random connections between clusters gives the fastest transport, but still does not outperform armchair nanotubes. This proved that highly regular graphs allow for faster continuous quantum walks. Future works could investigate the consequences of adding a simple potential as a model of defects, or simulating the dynamics of more particles on the same lattice. Finally, especially if real world applications are considered, a study on the effect of decoherence would provide very useful insights into the physics of quantum transport.

Acknowledgments

The author would like to thank Dr Vivien Kendon and Dr Nicholas Chancellor for their supervision, guidance and helpful discussions.

References

- [1] K. Pearson, The Problem of the Random Walk, *Nature*. 72, 294 (1905).
- [2] P. A. Gagniuc, *Markov Chains: From Theory to Implementation and Experimentation*, USA, NJ: John Wiley & Sons, 1–235 (2017).
- [3] Emanuel Parzen, *Stochastic Processes*, Courier Dover Publications, 188 (2015).
- [4] C. Papadimitriou, *Computational Complexity*, Addison Wesley, Reading, Massachusetts, (1994).

- [5] A. Sinclair, Algorithms for Random Generation and counting, a Markov Chain approach, Birkhauser press (1993).
- [6] Moore, Gordon E, Cramming more components onto integrated circuits, Electronics Magazine, 4 (1965).
- [7] R.J. Hughes, D.M. Alde, P. Dyer, G.G. Luther, G.L.Morgan, and M. Schauer, Quantum cryptography, *Contemp. Phys.*, 36(3):149–163 (1995).
- [8] P.W. Shor, Algorithms for quantum computation: Discrete log and factoring, S. Goldwasser, Proceedings of the 35th Annual Symposium on the Foundations of Computer Science, Los Alamitos, CA, IEEE Computer Society, 124–134 (1994).
- [9] Richard P. Feynman, Simulating Physics with Computers, *International Journal of Theoretical Physics*, Vol. 21, Nos. 6/7, (1982).
- [10] <https://www.research.ibm.com/ibm-q/> Date accessed: April 9th 2019.
- [11] A. Kandala, A. Mezzacapo, K. Temme, M. Takita, M. Brink, J. M. Chow & J. M. Gambetta, Hardware-efficient variational quantum eigensolver for small molecules and quantum magnets, *Nature* volume 549, 242–246 (2017).
- [12] L. K. Grover, Quantum mechanics helps in searching for a needle in a haystack, *Phys. Rev. Lett.* 79, 325 (1997).
- [13] R. P. Feynman, A. R. Hibbs, Quantum mechanics and path integrals, International series in pure and applied physics, McGraw-Hill, New York, (1965).
- [14] D. Meyer. From quantum cellular automata to quantum lattice gases. *J. Stat. Phys.*, 85:551–574, 1996.
- [15] E. Farhi and S. Gutmann, Quantum computation and decision trees, *Phys. Rev. A*, 58:915–928, 1998.
- [16] Frederick W. Strauch, Connecting the discrete and continuous-time quantum walks, *Phys. Rev. A* 74,030301 (2006).
- [17] A. Blumen O. Mülken, Continuous-time quantum walks: Models for coherent transport on complex networks. *Physics Reports*, 502, 37–87, (2011).
- [18] A. Ambainis, J. Kempe, and A. Rivosh, Coins make quantum walks faster, in Proceedings of the 16th Annual ACM-SIAM Symposium on Discrete Algorithms (Society for Industrial and Applied Mathematics, Philadelphia, PA), 1099 (2005).
- [19] A. M. Childs and J. Goldstone, Spatial search by quantum walk, *Phys. Rev. A* 70, 022314 (2004).
- [20] Iain Foulger, Sven Gnutzmann, and Gregor Tanner, Quantum walks and quantum search on graphene lattices, *Physical Review A* 91, 062323 (2015).
- [21] Vivien M. Kendon and Christino Tamon, Perfect state transfer in quantum walks on graphs, *J. Comp. Theor. Nanoscience* 8, 422–433 (2010).
- [22] S. Bose, Quantum communication through an unmodulated spin chain, *Phys. Rev. Lett.* 91, 207901 (2003).
- [23] F. Spitzer, Principles of random walk, Springer, 2nd edition, (1976).
- [24] R. Coleman, Stochastic Processes, George Allen & Unwin, Ltd, (1974).
- [25] P. G. Doyle and J.L. Snell, Random walks and electric networks, The Carus Math. Monographs (28), Mathematical Association of America, (1984).
- [26] J. Kempe, Quantum random walks - an introductory overview, *Contemporary Physics*, Vol. 44 (4),

p.307-327, (2003).

- [27] A. Ambainis, E. Bach, A. Nayak, A. Vishwanath, and J. Watrous, One-dimensional quantum walks, Proceedings of the 33rd ACM Symposium on The Theory of Computation (STOC'01) ACM, 60-69 (2001).
- [28] E. Bach, S. Coppersmith, M. P. Goldschen, R. Joynt, J. Watrous, One-dimensional quantum walks with absorbing boundaries, *J. Comput. Syst. Sci.* 69 (4), 562-592 (2004).
- [29] A. Ambainis, E. Bach, A. Nayak, A. Vishwanath, J. Watrous, One-dimensional quantum walks, Proc. 33rd Annual ACM STOC. ACM, NY, 60–69, (2001).
- [30] R. P. Feynman, R. B. Leighton, M. Sands, *Feynman Lectures on Physics*. Addison Wesley (1964).
- [31] A. Ahmadi, R. Belk, C. Tamon, C. Wendler, On mixing in continuous-time quantum walks on some circulant graphs, *Quantum Inform. Comput.* 3 (6), 611–618 (2003).
- [32] F. W. Strauch, Connecting the discrete and continuous-time quantum walks, *Phys. Rev. A*, 74:030301, 2006.
- [33] A. Childs, On the relationship between continuous- and discrete-time quantum walk, *Communications in Mathematical Physics*, vol. 294(2), 581-603, 2010.
- [34] Viv Kendon, Decoherence in quantum walks - a review, *Math. Struct. in Comp. Sci.* 17(6), 1169-1220 (2006).
- [35] K. S. Novoselov, A. K. Geim, S. V. Morozov, D. Jiang, Y. Zhang, S. V. Dubonos, I. V. Grigorieva, A. A. Firsov, Electric Field Effect in Atomically Thin Carbon Films, *Science*. 306 (5696), 666–669 (2004).
- [36] N. Hamada, S. Sawada, and A. Oshiyama, New one-dimensional conductors: Graphitic microtubules, *Phys. Rev. Lett.* 68, 1579 (1992).
- [37] C. Lee, X. Wei, J. W. Kysar, J. Hone, Measurement of the Elastic Properties and Intrinsic Strength of Monolayer Graphene, *Science* 321 (5887), 385–8 (2008).
- [38] Hamza Bougoura, Habib Aissaoui, Nicholas Chancellor, and Viv Kendon, Quantum walk transport properties on graphene structures, *Phys. Rev. A* 94, 062331 (2016).
- [39] Jean-Christophe Charlier, Xavier Blase, and Stephan Roche, Electronic and transport properties of nanotubes, *Rev. Mod. Phys.* 79, 677 (2007).
- [40] N. Hamada, S. Sawada, and A. Oshiyama, New one-dimensional conductors: Graphitic microtubules, *Phys. Rev. Lett.* 68, 1579 (1992).